Molecular reaction dynamics across the phases: similarities and differences

F. Fleming Crim*

Received 8th August 2012, Accepted 9th August 2012
DOI: 10.1039/c2fd20123b

This introduction to the 157th Faraday Discussion describes features of bimolecular reaction and photodissociation in gases and liquids and at interfaces. Two unifying ideas are the concepts of a transition state on a single potential energy surface and of a conical intersection between two surfaces, the former being important in bimolecular reactions and the latter often being important in photodissociation. State-resolved studies of the reactions of methane and its isotopologues with F, Cl, and Br illustrate many aspects of bimolecular reactions including the ability of excitation in vibrational modes to enhance or inhibit a reaction and to control the cleavage of selected bonds. There are clear parallels between those gas-phase reactions and the dissociative chemisorption of methane and its isotopologues on metal surfaces. Similarly, features such as relative reaction rates and energy disposal patterns observed in gas-phase reactions largely carry over into reactions in solution. New experiments comparing photolysis in the gas phase and in solution show that there are again many similarities in the processes in the two environments. Although the influence of the surroundings in those cases is subtle, there are situations in which the surroundings can produce a much larger effect on the photolysis by hindering the dissociation and initiating isomerization.

1. Introduction

A Faraday Discussion with the expansive topic of *Molecular Reaction Dynamics in Gases*, *Liquids*, *and Interfaces* involves diverse aspects of chemical transformations, and, fortunately, a few organizing principles unite those strands. One is the notion that many chemical transformations occur through a transition state, a high energy configuration along the pathway between reactants and products. Another principle, which has come to the fore more recently, is the idea that excited state reactions, such as photodissociation and photoisomerization, often involve geometries in which two different electronic states form a conical intersection. Viewed in the proper coordinate system, this conical intersection is a special point at which the two states are degenerate but away from which they have different energies.[1] As with a transition state, the motion of the molecule in the vicinity of a conical intersection often controls the dynamics of the reaction.

Understanding the motion that carries a system through those special configurations and the consequences of that motion for energy consumption and disposal lies at the heart of molecular reaction dynamics. This introduction to the Discussion presents examples of reactions in gases and liquids and at interfaces with an eye toward identifying the similarities and differences among them. We examine

Department of Chemistry, University of Wisconsin - Madison, Madison, Wisconsin 53706, USA. E-mail: fcrim@chem.wisc.edu

separately the dynamics of bimolecular reactions and of photodissociation, both of which appear prominently in the articles and commentary in this Discussion.

2. Bimolecular reaction

The influence of the surroundings is the essential difference between reactions in gases and those in liquids and at interfaces. Interactions with the surroundings potentially alter the relative energies of the reactants, the products, and, perhaps most important, the transition state.

Fig. 1 illustrates three cases. In the first case, shown in Fig. 1(a), the solid curve is the energy along the reaction coordinate for a gas-phase reaction of two molecules. The dashed blue curve is an energy profile for a reaction in solution. It shows a slight stabilization of the reactants and products along with a greater stabilization of the transition state by the surrounding solvent. The result is a lower energy barrier to the reaction because of the greater stabilization of the transition state. The essential

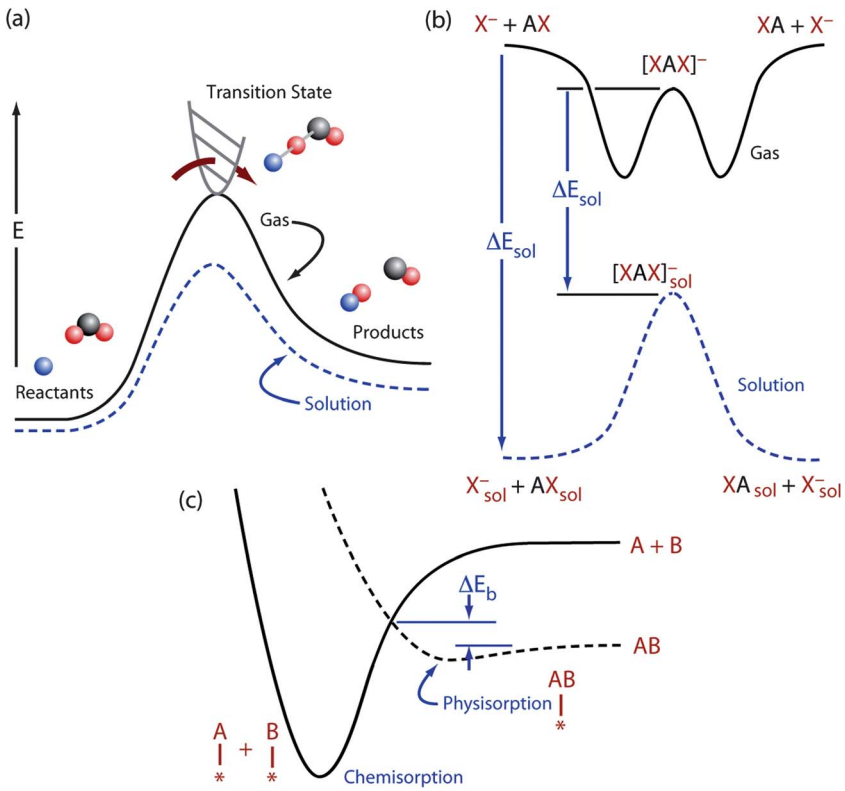

Fig. 1 (a) Energy profiles for a bimolecular reaction in the gas phase (solid black curve) and for a reaction in a liquid (dashed blue curve). In this example, the solvent lowers the energy of the reactants and products slightly but stabilizes the transition state by a larger amount. (b) Energy profiles for a gas-phase bimolecular ion-molecule reaction (solid black curve) and for the same ion-molecule reaction in a liquid (dashed blue curve). The transition state lies below the asymptotes in the gas phase, and there are bound minima along the reaction coordinate. The solvent stabilizes the reactants and products much more than the transition state, producing a very different energy profile in solution. (c) Potential energy curves for physisorption and dissociative chemisorption of the reactant AB. Reaction can occur by physisorption of the precursor AB followed by dissociation from that shallow well to form strongly bound A and B species on the surface. The minimum energy required is ΔE_b.

shape of the curve remains the same with small, but potentially significant, changes in the overall energetics. Another factor that is not obvious from examining the reaction profile alone is the role that the solvent might play in limiting motion through the transition state or redistributing energy in the reactants and products, ideas that enter into more sophisticated models of reaction in solution.[2,3]

The situation is very different for the symmetric ion-molecule reaction having the energy profile in Fig. 1(b). The solid curve has a deep attractive well as the ion approaches the molecule. In this example, the entrance-channel complex is so strongly bound that it "submerges" the transition state below the energy of the reactants and products. However, solvation changes the situation dramatically by stabilizing the reacting anion, X^-, much more that the transition state, as the dashed blue curve shows. The distribution of the charge over more atoms makes the solvent stabilization of the transition state smaller than that of the reactants. Interaction with the surroundings removes the entrance-channel well and produces a more conventional profile with the transition state lying well above the energy of the reactants and products.

The one-dimensional profiles shown in Fig. 1 are minimum energy paths across a multidimensional potential energy hypersurface, and the topology of that surface is critically important to energy consumption and disposal. The concepts of late and earlier barriers along with the kinematic effects of different mass combinations are another central organizing principle in molecular reaction dynamics.[4] These ideas are touchstones for this Discussion, and testing their limits in larger systems is a current theme in molecular reaction dynamics.

Descriptions of reactions at interfaces often use these same ideas, and surface reactions present other potential environmental effects as well. The two potential energy curves shown in Fig. 1(c) illustrate the simplest role that the surface can play. The dashed curve shows the energy profile for physisorption of the AB molecule in a shallow well, and the solid curve shows the energetics for dissociative chemisorption into two surface bound species A and B, which correlate to high energy dissociated fragments in the gas phase. Thus, the physisorbed molecule is a potential precursor in the dissociative chemisorption reaction, and the energy required to move from one region to another is the effective barrier, E_b, in this simple example. However, there may be larger barriers associated with the dissociation, and the reaction could involve displacement of surface atoms as well as changing the geometry of the dissociating molecule.

2.1 Gas-phase reactions: the CH_4 poster child

Abstraction of a hydrogen atom from the simplest alkane, CH_4, and its partially deuterated isotopologues illustrates varied aspects of molecular reaction dynamics,[5] and there are several examples in this Discussion. Fig. 2 shows the energetics for the abstraction of a hydrogen atom from methane to form a hydrogen halide and a methyl radical

$$X + CH_4 \rightarrow HX + CH_3$$

which vary dramatically with the identity of the halogen atom, X. The strong HF bond makes the reaction to form HF exothermic by 11 150cm^{-1} (133 kJ mol^{-1}), but the reaction to form HCl is modestly endothermic by 500 cm^{-1} (6 kJ mol^{-1}). By contrast, the still weaker HBr bond makes that reaction endothermic by 4300 cm^{-1} (50 kJ mol^{-1}). Thus, this series of reactions offers the possibility of examining both the consumption of energy in bond- and mode-selective reactions and the disposal of energy into product vibrations. Correlations between barrier location and thermochemistry show that exothermic reactions typically have early barriers (reactant-like transition states) and endothermic reactions typically have late barriers (product-like transition states). For triatomic systems, translational energy

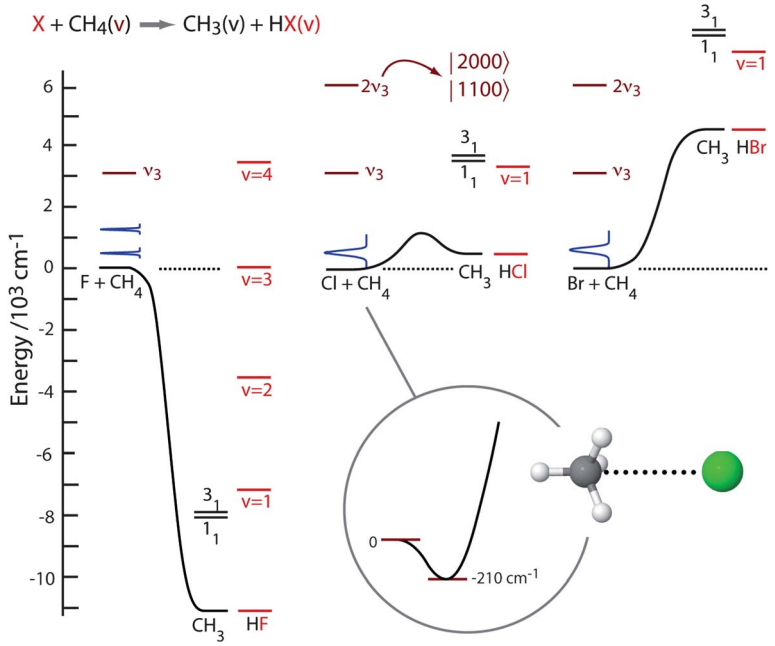

Fig. 2 Energetics for the reaction of a halogen atom with CH_4. The horizontal lines indicate the energies of the symmetric C–H stretching states (ν_3) of CH_4 (dark red), the energy levels of the symmetric and antisymmetric C–H stretching states (1_1 and 3_1) of CH_3 (black), and the vibrational levels of the hydrogen halide HX (red). The inset shows the calculated van der Waals minimum for the case of Cl + CH_4. There are similar minima for all three reactions.

promotes reaction most effectively in the former case and vibrational energy in the latter case.[4] The inset in Fig. 2 illustrates another potentially important feature of these reactions, the presence of a shallow van der Waals well in the entrance channel. Its calculated depth[6] is about 210 cm^{-1} for the case of chlorine shown in the figure, and the well depth is more than 100 cm^{-1} for each of these reactions.[7]

The energy available for populating different product states differs markedly for the three reactions. There is enough energy available in the reaction with F to populate vibrational states of HF up to $v = 3$ or to excite the CH_3 product to high vibrational states. Fig. 2 shows the energies of only the two lowest C–H stretching states of methyl, the symmetric C–H stretch ν_1 and the anti-symmetric C–H stretch ν_3, indicated by the notation 1_1 and 3_1. The endothermic reactions of CH_4 with Cl and Br cannot produce vibrationally excited products without additional translational or vibrational energy in the reactants.

There are now examples of all three of these atoms reacting with vibrationally excited methane,[8–11] and the figure shows the energies of CH_4 reactants containing one (ν_3) and two quanta ($2\nu_3$) of antisymmetric C–H stretching excitation. Initial excitation of two quanta of C–H stretch, as shown for the Cl and Br reactions, introduces an additional aspect of initial state preparation. It is possible to excite eigenstates corresponding to either one quantum of excitation in each of two bonds, the $|1100\rangle$ state in local-mode notation,[12,13] or two quanta in one bond, the $|2000\rangle$ state. As described below, these initial states react differently despite being very close in energy, an example of vibrational-mode-selective chemistry.

2.1.1 Translational energy. Translational energy allows reactions to surmount the energy barrier, as in the case of Cl and Br reactions with CH_4, or provides energy to populate higher lying product states, as in the case of the exothermic reaction of F

with CH_4. The barrier for the reaction of Cl is low enough that a relatively small amount of translational energy from photolysis of a precursor can overcome it. The reaction of translationally energized Cl atoms with a methane isotopologue, CH_3D, illustrates this behaviour. The reaction has two channels, abstraction of either H or D,

$$Cl + CH_3D \rightarrow DCl + CH_3$$
$$Cl + CH_3D \rightarrow HCl + CH_2D$$

that have different energy barriers arising from the difference in the zero-point energy of the C–H and C–D bonds. At the transition state, the bond that breaks is unbound and, thus, has no zero-point energy. Consequently, the transition state for breaking a C–H bond, with its larger zero-point energy, lies lower than that for breaking a C–D bond because the zero-point energy "disappears" in the transition state. This difference in barrier heights is the origin of the primary kinetic isotope effect, and Fig. 3(a) shows the relative size of the barriers for the two channels in the reaction of Cl with CH_3D.

The figure illustrates the approach we use for studying the role of both translational and vibrational energy in the reaction.[14–16] These experiments photolyze Cl_2

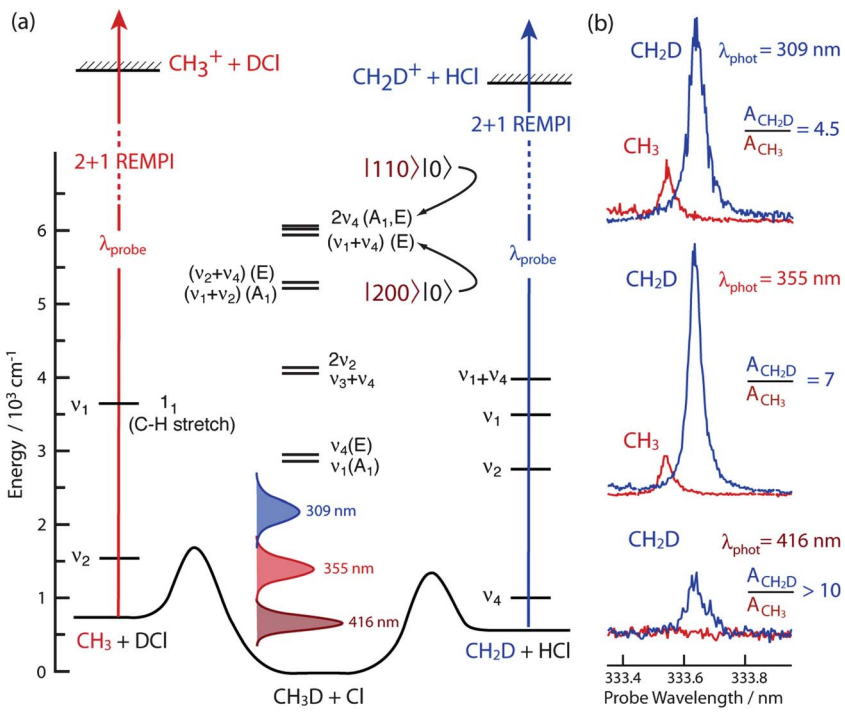

Fig. 3 (a) Energy profile along the reaction coordinates for Cl reacting with CH_3D to produce either CH_3 + DCl or CH_2D + HCl showing vibrational levels of CH_3D as well as vibrational levels of the CH_3 or CH_2D products detected by (2+1) REMPI. The distributions show the relative translation energy in the system following photolysis of Cl_2 with 416 nm (dark red), 355 nm (red), or 309 nm (blue) light. (b) Relative REMPI signals for the CH_2D product (blue) and the CH_3 (red) product at each photolysis wavelength. The relative amount of the CH_2D product grows as the translational energy decreases. At the lowest energy, the CH_3 is undetectable.

to generate Cl atoms in a free-jet expansion that also contains CH_3D, and they monitor individual vibrational states of both the CH_2D and CH_3 reaction products by resonance enhanced multiphoton ionization (REMPI). In these (2+1) REMPI measurements, two photons excite a resonant intermediate state, and another photon ionizes the molecule for detection in a time-of-flight mass spectrometer. As described below, it is also possible to excite the vibrational eigenstates of CH_3D shown in the diagram in order to observe the influence of vibrational excitation on the course of the reaction. First we consider the influence of translational energy alone.

The three distributions in Fig. 3(a) show the relative translational energy, E, between Cl and CH_3D for photolysis of Cl_2 with three different wavelengths of light.[17] Photolysis with 416-nm light gives a most probable relative translational energy of $E_{416} = 610\ cm^{-1}$, photolysis with 355-nm light gives $1280\ cm^{-1}$, and photolysis with 309-nm light gives $1970\ cm^{-1}$.[18] This threefold change in energy alters the branching between the two channels substantially, as Fig. 3(b) shows. The curves are the REMPI signals as a function of the probe wavelength for the CH_3 product (red) and the CH_2D product (blue). At the highest energy ($\lambda_{phot} = 309$ nm), the area of the CH_2D signal is about 4.5 times larger than that of CH_3, but it increases to 7 times larger for the next lower energy photolysis ($\lambda_{phot} = 355$ nm). At the lowest photolysis energy ($\lambda_{phot} = 416$ nm), we observe only the CH_2D product. These variations suggest that the lowest energy photolysis places the system well below the barrier to breaking the C–D bond (to produce CH_3) and that the highest energy photolysis places the system above both barriers.

This conclusion is consistent with a calculation by Cazko, *et al.*[6] that finds the barrier to cleaving the C–H bond in the Cl + CH_4 reaction to be about $1200\ cm^{-1}$. Correcting that value by the $360\ cm^{-1}$ difference in zero-point energies of a C–H and a C–D bond gives an estimate of $1560\ cm^{-1}$ for the height of the barrier to cleaving the C–D bond, as shown in the figure. Thus, we expect that few, if any, of the collisions carry the system over the barrier at the lowest translational energy ($610\ cm^{-1}$). It is likely that H-atom tunnelling is the dominant pathway in that case and that reaction to cleave the C–D bond is negligible. At the next higher translational energy ($1280\ cm^{-1}$), a sizeable fraction of the collisions have enough energy to pass over the barrier to breaking the C–H bond, but only a few have enough to surmount the barrier for breaking the C–D bond. The CH_3 products likely come from tunnelling while the CH_2D products come primarily from reaction over the barrier. Finally, at the highest translational energy both channels are open, and the observed ratio of products is consistent with statistical partitioning between the two channels.[17,19]

2.1.2 Vibrational energy. Vibration is another degree-of-freedom available for initial excitation in the methane reactant. The reaction of F with CH_4 provides a striking example of the influence that vibrational energy can have even on a very exothermic reaction. In this Discussion, Kawamata, *et al.* detect the CH_3 fragment from the reaction using ion imaging and infer the energy content of the unobserved HF product.[8] They find HF vibrational states populated up to the energetic limit shown in Fig. 2. Most significantly, however, they observe that excitation of the antisymmetric C–H stretch (ν_3) in CH_4 *inhibits* the C–H bond cleavage. When reaction does occur, it preserves the vibration and forms CH_3 with a quantum of C–H stretch excitation. The authors suggest that the transition state in this early-barrier reaction resembles the reactants and that a geometry with a stretched C–H bond does not lie along the minimum energy path.

Reactions of Cl with methane and its isotopologues have provided clear examples of both mode- and bond-selected chemistry in which vibrational excitation directs the reaction along a particular course.[5] Although there are some subtleties, two general trends emerge from studies of all the isotopologues. One is that exciting an eigenstate with substantial C–H or C–D stretching character in a mixed

isotopologue leads to preferential cleavage of that bond.[15] The other is that the bonds that do not break largely act as spectators, preserving their initial excitation in the products.[20,21] As the energy level diagram for CH_3D in Fig. 3(a) shows, one quantum of C–H stretching excitation (ν_1 or ν_4) places the system above the barrier, and in most cases, there is significant translational energy from the photolysis as well. Even though there is background reaction from translationally energized molecules without vibrational excitation, adding vibrational excitation increases the reaction cross section markedly. However, reactive scattering experiments in CHD_3 show that vibration is no more effective than an equivalent amount of energy in translation.[22] Both forms of energy accelerate the reaction, but only vibrational excitation controls the outcome.

The reaction of CH_3D with Cl also illustrates mode-selective reaction. Exciting the symmetric C–H stretch (ν_1) or the antisymmetric C–H stretch (ν_4) leads to preferential cleavage of the C–H bond to produce CH_2D, as illustrated in Fig. 3(a). Vibrational action spectra obtained by monitoring the CH_2D product show that molecules with the symmetric stretching mode excited are about six times more reactive than those with the antisymmetric mode excited, even though the two states differ primarily in the phase of their vibrations and lie within 100 cm^{-1} of each other. The key to this mode selectivity is the evolution of the initially excited eigenstate during the collision.[16]

The bond selectivity and the spectator behaviour of the surviving bonds shows that the perturbation of the incoming Cl atom does not mix the vibrational states extensively although it changes the relative reactivity of the two states. Models of the interaction of vibrationally excited water with Cl[23] and of vibrationally excited methane with a Ni surface[24] as well as more detailed electronic structure calculations of the interaction of Cl with CH_3D[16] provide a picture of the evolution of the initially excited state. As a Cl atom approaches a CH_3D molecule along a C–H bond, the symmetric stretching vibration changes from the movement of all three atoms together to the vibration of the bond directed toward the incoming Cl. By contrast, the antisymmetric stretching vibration evolves into motion of the two C–H bonds directed away from the incoming atom, making that vibration less reactive. In fact, there is a relatively simple symmetry argument that leads to this outcome for approach along a C–H bond.[16] This result points to the importance not only of the nature of the initially prepared vibrations but also of their evolution during the reaction. Even in the absence of extensive state mixing (collision induced intramolecular energy redistribution), excited states can evolve in subtle ways that alter their reactivity.

The reaction of CH_4 with Br is another example of mode selectivity that is strongly reminiscent of the first examples of such behaviour in the reaction of H or Cl with H_2O.[25–27] As Fig. 2(c) shows, one quantum of C–H stretching excitation provides too little energy to surmount the barrier, and, even with an additional 1300 cm^{-1} of translational energy, the total energy is barely enough for the reaction to occur. However, two quanta of excitation in the antisymmetric stretch ($2\nu_3$) provide enough energy for the reaction. As described above, there are two spectroscopically distinct transitions in the $2\nu_3$ region that excite either the local-mode state containing one quantum in each of two different C–H bonds, $|1100\rangle$, or the one with two quanta in one C–H bond, $|2000\rangle$. In the former case, there is not enough energy in either bond to overcome the barrier, and we observe no reaction.[11,19] In the later case, however, we observe reaction to produce ground vibrational state methyl radicals. This mode-selective reaction is another manifestation of the independence of the potentially reacting bonds. There is not enough energy in any single bond to overcome the reaction barrier even though there is enough energy in the molecule. Because the interaction with the Br atom does not transfer energy between the bonds, only the state that initially has its vibrational energy in a single bond reacts. This behaviour is the other side of the spectator picture in which the reacting bond does not communicate with the non-reacting bond.

2.2 Reactions in solution: H-atom abstraction

Transferring bimolecular, gas-phase reactions into solution presents challenges and opportunities. A molecule in a gas at a pressure of 1 Torr collides roughly every 100 ns, but in a gas having the density of a liquid, a molecule collides every 100 fs. Thus, observing events on the timescale of the interval between interactions requires time resolution of about 100 fs. Consequently, one must trade the high spectral resolution possible in gas-phase measurements for high time resolution in liquid-phase experiments. However, it is still possible to observe populations in different vibrational states in favourable cases and to answer some of the same questions that gas-phase molecular reaction dynamics explores.

Hydrogen-atom abstraction reactions from alkanes and substituted alkanes

$$X + RH \rightarrow HX + R\cdot$$

are attractive targets for which there are some gas-phase data for comparison. In the gas-phase measurements on CH_4 described above, quantum-state resolved detection of the methyl radical is a key. In solution, it is possible to follow the reaction using transient absorption of the HX product, and pioneering experiments by Hochstrasser first used that approach.[28,29] These experiments produce a reactive radical photolytically and monitor the reaction product with transient infrared absorption. Changing the identity of the attacking species makes the range of thermochemistry shown in Fig. 2 potentially available for such reactions, but hydrogen atom abstraction by Cl and by CN are the two most extensively studied examples. In the first experiments, Hochstrasser studied the reactions of Cl with cyclohexane[28] and CN with chloroform,[29] and the CN reactions showed the first evidence of vibrationally excited products in the case of deuterochloroform. More recent experiments have built on those studies.

It is also possible to follow a reaction by observing the loss of one of the reactants. Fig. 4(a) shows a scheme for an experiment probing either the loss of the Cl reactant or the formation of the HCl product in the reaction of Cl with an alkane.[30] After photolyzing Cl_2 with a pulse of 350 nm light, we probe the Cl atom, which forms a weakly bound complex with the solvent, with a 330 nm pulse that excites the strongly bound charge-transfer state. Monitoring this transient absorption as a function of the delay between the photolysis and probe pulse for the reaction of pentane with Cl in a CH_2Cl_2 solution yields the decay curves shown in the top part of Fig. 4(b). The decay is faster for larger pentane concentrations, and the concentration dependence of the decay yields the bimolecular rate constant. Similarly, it is possible to monitor the ground-vibrational-state HCl product by transient absorption of a 3.6 μm infrared pulse. The growth of that signal, shown in the bottom of Fig. 4(b), exactly mirrors the decay of the Cl atom.

A set of experiments probing the loss of Cl in reactions with alkanes, alcohols, and chloroalkanes provides a set of rate constants for comparison to gas-phase results.[31] The alkanes react at the diffusion limited rate, but the alcohols have a slightly smaller rate, reflecting a small activation barrier for the reaction. However, the chloroalkanes provide the most informative comparison with the rates of gas-phase reactions. The reaction rates for the chloroalkanes vary from nearly diffusion-limited to almost an order-of-magnitude slower, reflecting the changes in the barrier to reaction with increasing substitution. There are structure–activity relationships for reactions of the chloroalkanes with Cl developed for modelling the rates of atmospheric reactions.[32,33] These gas-phase rules reproduce the relative reaction rates in solution very well,[31] showing that the variation of the activation energy among the reactants in solution follows that in the gas phase. Thus, it seems that the gas-phase relative reaction rates are a sound predictor of the relative rates in solution, at least in the weakly interacting solvent we used.

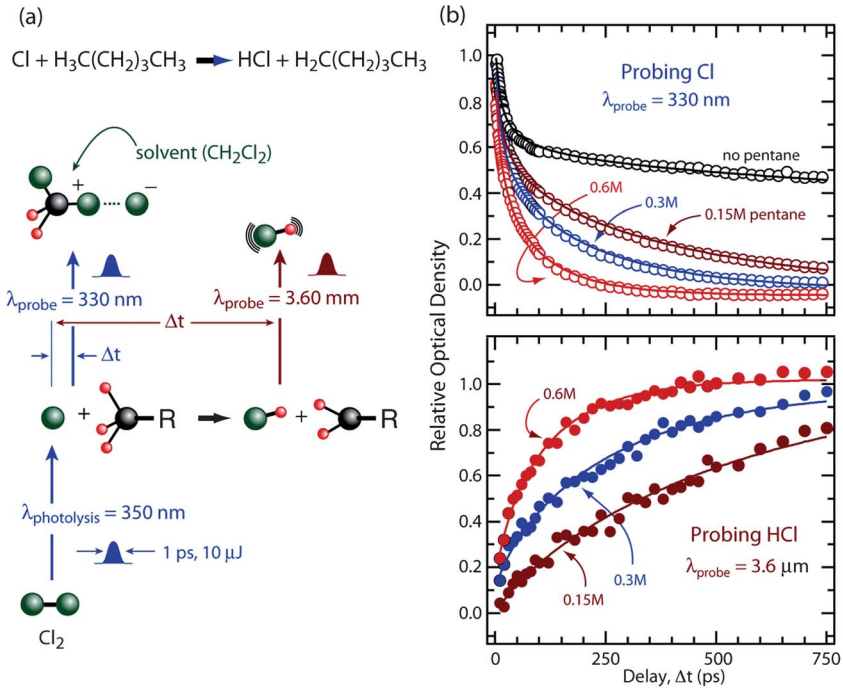

Fig. 4 (a) Scheme for time-resolved study of the bimolecular reaction of Cl with an alkane in solution. Photolysis of Cl_2 generates Cl atoms that react with pentane in CH_2Cl_2 solution, and transient absorption of the Cl-solvent complex to a charge-transfer state follows the evolution of the Cl atom. A short infrared pulse follows the appearance of the HCl product of the H-atom abstraction reaction. (b) Time-evolution of the Cl reactant (top) and HCl product (bottom).

The reactions of CN with alkanes are perhaps an even more interesting possibility for comparison because the stronger H–CN bond makes the reaction exothermic enough to excite vibrations of the product, as studies of CN reactions in the gas phase demonstrate.[34–36] Recent experiments by Orr-Ewing and coworkers use broad-band infrared detection of the HCN formed in the reaction of photolytically produced CN radicals in solution.[37,38] Fig. 5 shows the results of their measurements on the reaction of CN with cyclohexane

$$CN + c\text{-}C_6H_{12} \rightarrow HCN(v_1\ v_2\ v_3) + c\text{-}C_6H_{11}.$$

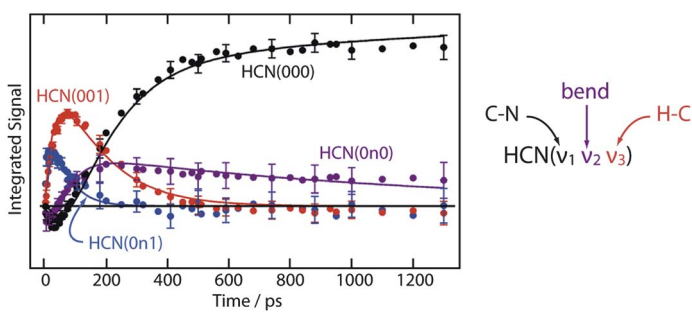

Fig. 5 Time evolution of vibrational-state populations of HCN formed in the reaction of CN with cyclohexane in dichloromethane solution. The vibrationally excited products, HCN(001) and HCN(0*n*1) appear initially. Subsequent vibrational relaxation populates the ground vibrational states. (Adapted from ref. 37 with permission of AAAS.)

The vibrational quantum numbers of HCN denoting the three normal modes correspond to the C–N stretch (ν_1), the HCN bend (ν_2), and the C–H stretch (ν_3). The time-resolved, broadband infrared spectra show that the reaction initially forms HCN with an excited C–H stretch along with some bending excitation. The time-evolution of each of those states shown in Fig. 5 clearly demonstrates the evolution of the vibrationally excited HCN. Both stretch-excited products, HCN(001), and stretch-bend-excited products, HCN(0n1), appear in the first 60 ps. Vibrational relaxation eventually moves molecules into the ground state, HCN(000), over about 200 ps. Previous measurements assigned this time constant to reaction,[29,39] but it is clear that those experiments observed vibrational relaxation after a much faster reaction, a cautionary point for studies of nascent products in solution.

These experiments provide a comparison of reaction dynamics in solution, not just rates, with those in gases. The initial production of vibrationally excited molecules is consistent with the observations in gases although the gas-phase reaction produces higher levels of excitation. Clearly the presence of the solvent does not alter the energy release dramatically but rather makes more subtle differences in the course of the reaction.[37,38] A combination of experimental advances and new insights is opening the door to studies of molecular reaction dynamics in solution.

2.3 Reactions on metal surfaces: the CH_4 poster child redux

The dissociative chemisorption of methane on a metal surface

$$CH_4 \rightarrow CH_3(ads) + H(ads)$$

offers the possibility of observing mode- and bond-selective chemistry in yet another environment, and there are striking parallels with the reaction dynamics in the gas phase. Elegant surface scattering experiments using molecular beams of vibrationally excited methane and its isotopologues[40–53] have established the relative efficacy of translational and vibrational energy in promoting the dissociation and have demonstrated both mode- and bond-selective reactions of vibrationally excited molecules. For example, in the case of methane on Ni(100),[48] the symmetric stretching vibration (ν_1) promotes dissociative adsorption about ten times more effectively than the antisymmetric stretching vibration (ν_3). In addition, these experiments show that translational energy normal to the surface also enhances the reaction. A translational energy increment of about 50 kJ mol^{-1} increases the probability of dissociative chemisorption as effectively as the 36 kJ mol^{-1} of vibrational energy provided by excitation of the symmetric stretch. Both the mode-selectivity and the effect of increased translational energy parallel the behaviour described above for single collision reactions of methane with Cl.

There are parallels in the bond-selectivity of the gas-phase and surface reactions as well. The first demonstration of bond-selective dissociative chemisorption used the reaction of subsurface D atoms with the chemisorbed species to show the preferential cleavage of the initially excited bond in CHD_3 on a Ni(111) surface.[45] In these experiments, CHD_3 molecules with an initially excited C–H stretching vibration always dissociate to leave CD_3 radicals on the surface, as shown by the exclusive production of CD_4 in reaction with the subsurface D atoms. An extensive study presented in this Discussion[54] expands the scope of experiments on bond-selective dissociative chemisorption by using Reflection Absorption Infrared Spectroscopy (RAIRS) to interrogate the species on the surface after dissociative chemisorption of methane and its isotopologues. The generality of this surface spectroscopy allows Beck and coworkers to examine the entire series of methane molecules with increasing deuteration: CH_4, CH_3D, CH_2D_2, CHD_3, and CD_4. Fig. 6 shows a portion of one of their RAIRS spectra comparing the absorbed species produced from CH_3D without vibrational excitation (lower trace) to those from CH_3D with C–H stretching excitation (upper trace). The data show that chemisorption cleaves

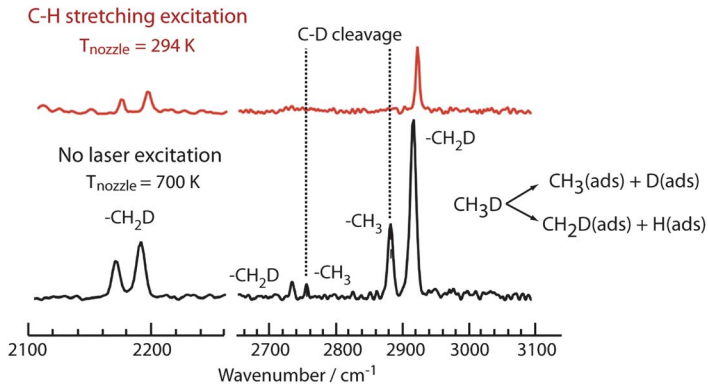

Fig. 6 Reflection Absorption Infrared Spectra (RAIRS) of adsorbed species on Pt(111) from dissociative chemisorption of CH_3D with energy in translation (bottom trace, black) or in C–H stretching vibration (top trace, red). Translational energy causes both the C–H and C–D bonds to break, but vibrational excitation of the C–H stretch leads solely to cleavage of that bond. (Adapted from ref. 54 with permission of the Royal Society of Chemistry.)

only the C–H bond when it is initially vibrationally excited but that both the C–H and C–D bonds break when the energy is in relative translation.

These experiments "ring the changes" on all of the isotopologues and paint a consistent picture of the effect of vibrational excitation, showing that dissociative chemisorption cleaves the vibrationally excited bond, in analogy to bimolecular gas-phase reactions. The interaction with the surface is complicated, and these detailed results present a challenge to theory in understanding the evolution of the excited molecule as it approaches the surface and the nature of the transition state through which the reaction occurs. It seems likely that the evolution of the excited state during the interaction with the surface has much in common with the evolution as the vibrationally excited molecule approaches an atom in the gas phase.

3. Photodissociation

Electronic photodissociation involves promoting a molecule to an excited electronic state from which it either dissociates directly or on which it evolves to reach another electronic state from which it dissociates. As described in the introduction, some of the most important regions on the excited-state surface are those where two electronic states having the same energy form a conical intersection. Conical intersections have emerged as a unifying idea in excited state chemistry.[55–58] Fig. 7 shows one-dimensional cuts through the potential energy surfaces of several molecules in which conical intersections are important. As the figure shows, multiple surfaces can participate, and, in all of these cases, there is one state in which excitation into an antibonding orbital initiates the excited state dynamics.

3.1 Conical intersections and product states

Moving an electron into a σ* orbital in ammonia makes the system dissociative along the N–H coordinate, as shown in Fig. 7(a). Interactions with higher-lying states create an excited-state barrier, and beyond that barrier the excited state falls in energy to correlate with ground-state NH_2 and H fragments. Along the way, it crosses the ground state of NH_3, which correlates with excited-state NH_2, and this crossing forms a conical intersection. The surfaces in Fig. 8 show the structure along two coordinates, one N–H bond length, R, and the umbrella bending coordinate, θ. The barrier between the two pyramidal minima in the ground electronic state is at

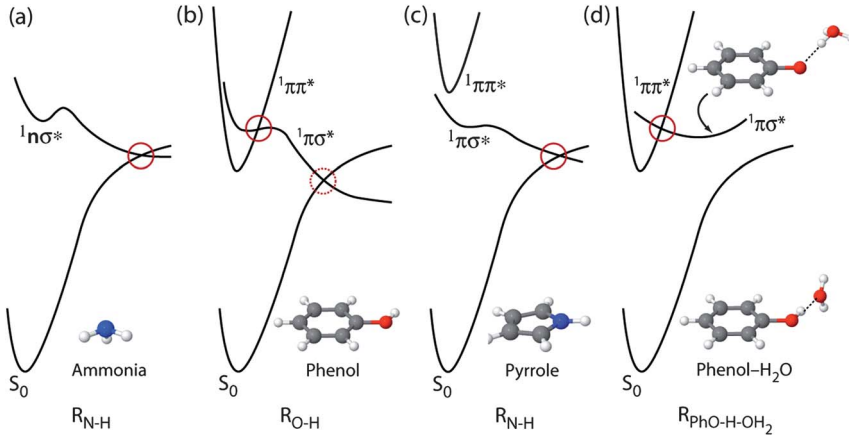

Fig. 7 Potential energy curves for (a) ammonia, (b) pyrrole, (c) phenol, and (d) the phenol-water complex. The red circles mark the conical intersections in each system.

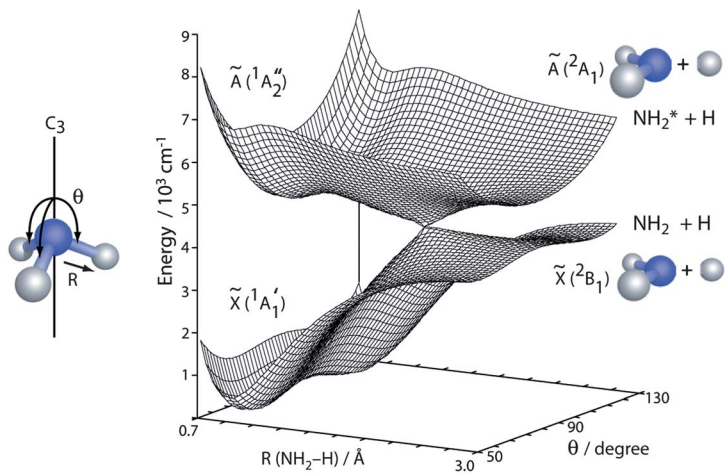

Fig. 8 Calculated ground- and first excited-state potentials of ammonia. The coordinates are R, the distance along one of the N–H bonds, and the angle, θ, the out-of-plane bending angle.

the planar geometry, $\theta = 90°$, and motion along that coordinate is the familiar inversion tunnelling. In planar ammonia, the excited state and the ground state, which correlate with different electronic states of the products, do not interact because they have different symmetries. However, in non-planar geometries, they do interact because their symmetries are the same. The two adiabatic states separate in energy, forming the conical intersection shown in the figure, which is particularly easy to see along these coordinates. A more general description uses two different coordinates that are not always so easy to identify in terms of bond coordinates.[1,56,58] However, locating the conical intersection constrains only those two coordinates and leaves the others free.

The curves for phenol in Fig. 7(b) illustrate a recurring theme in the excited state dynamics of heteroaromatic molecules.[59] Both excited states involve the promotion of an electron from the bonding π orbital of the aromatic ring, but they differ in the destination orbital. The ππ* state has that electron in the antibonding pi orbital,

and the $\pi\sigma^*$ state has that electron in an antibonding sigma orbital. The transition to the $\pi\pi^*$ state is generally stronger (the transition to the $\pi\sigma^*$ state is symmetry forbidden in benzene), and in many cases vibronic coupling of the two states provides the oscillator strength for the transition to the $\pi\sigma^*$ state. The curves for phenol have two conical intersections, one between the two excited states, $\pi\pi^*$ and $\pi\sigma^*$, and one between the $\pi\sigma^*$ state and the ground state S_0. The branching between the states at each of these intersections is critical in the dissociation dynamics.[58,60] It determines the populations of the electronic states of the dissociation products, as revealed, for example, by high resolution, H-atom Rydberg state time-of-flight measurements.[59]

The curves for pyrrole in Fig. 7(c) illustrate a different situation involving the same three states. In this case, the location of the $\pi\pi^*$ state at an energy well above that of the $\pi\sigma^*$ state removes one of the conical intersections, and excitation of the $\pi\pi^*$ state does not lead directly to the intersection and dissociation on the $\pi\sigma^*$ state. Thus, the relative energies of these interacting states is a controlling feature of the photodissociation that explains trends among various molecules.[59]

It is also possible to alter the relative energies of the states by interaction with an adduct, as the calculated potentials for the complex of phenol with water[61] shown in Fig. 7(d) illustrate. A single hydrogen-bonded water molecule alters the energy of the $\pi\sigma^*$ state to remove the intersection between that state and the ground state. In fact, there is stable minimum on the $\pi\sigma^*$ state in which the hydrogen atom resides on the water molecule. This change in the excited-state potential raises the possibility that the surroundings could alter dissociation pathways substantially in solution by changing the energies of interacting excited states, a possibility that experiments are beginning to explore.[62]

3.2 Dissociation of isolated molecules and the influence of vibrations

There is a rich history of probing asymptotic product states, using techniques such as Rydberg tagging and ion imaging, to infer details of the dissociation dynamics. One of the keys is detecting one product in a specific state with sufficient speed resolution to infer the distribution of the unobserved products among their quantum states. For example, in this Discussion, Kable and coworkers describe experiments using ion imaging to study the three-body dissociation of acetaldehyde.[63]

A means of influencing excited-state dynamics is to prepare a molecule on the excited state with selected initial nuclear motions. Exciting vibrations in ground-state molecules brings new Franck–Condon factors into play and permits excitation to new regions of the excited-state surface. Early experiments show that these schemes can control the cleavage of a selected bond in HOD, for example.[64] The photodissociation of vibrationally excited ammonia molecules even makes it possible to influence the relative yield of ground-state and excited-state NH_2 products, reflecting the branching between the two states at conical intersections.[65,66]

The experiments on the photodissociation of vibrationally excited ammonia prepare NH_3 molecules with either a quantum of symmetric N–H stretching excitation or a quantum of antisymmetric N–H stretching excitation. As Fig. 8 shows, formation of ground-state ($^2B_1$) NH_2 products makes about 10 000 cm^{-1} more energy available than formation of excited-state ($^2A_1$) NH_2. In the latter case, the extra energy resides in electronic excitation of the product. Experiments detecting the translational energy of the products show that photodissociation of molecules from the antisymmetric N–H stretching state forms slowly recoiling H atoms and suggest that the partner is the electronically excited product NH_2^*.[65] Ion imaging experiments confirmed this supposition by detecting the recoiling H atoms with sufficient speed resolution to show the undetected NH_2 product has the rotational state structure of NH_2^*.[66]

The situation for photodissociation from the symmetric N–H stretching state is very different. The H-atom recoil distribution shows that photolysis forms NH_2 in

its ground electronic state with a kinetic-energy distribution that is very similar to that for photolysis of ground-state NH_3. Thus, only initial excitation of the antisymmetric stretching vibration promotes the adiabatic decomposition in which the dissociation evolves on the upper surface. Theoretical calculations show that in the excited state the antisymmetric N–H stretching vibration carries the system away from the conical intersection shown in Fig. 8 towards another one where non-adiabatic transitions to the lower surface are less efficient. This behaviour in part comes from the development of angular momentum in the vibrationally excited molecule.[67] These experiments show that exploring different parts of the excited-state surface can substantially alter the decomposition dynamics in systems with conical intersections. Measurements show a similar, but less dramatic, effect in the decomposition of vibrationally excited phenol.[68]

3.3 Photodissociation in solution

3.3.1 Dissociation of prototypical aromatic molecules in solution. Several aromatic molecules are prototypes because of their conical intersections, illustrated in Fig. 7, and because of the detailed gas-phase studies by Ashfold and coworkers.[59] Thus, they are good targets for photodissociation in solution, and in this Discussion, Bradforth, Ashfold, and coworkers present such a ground breaking, time-resolved experiment.[62] As described above, observing the early time dynamics of the decomposition in solution relies on good time resolution rather than the high energy resolution used in gas-phase studies. They study the photodissociation of isolated phenol and *p*-methylthiophenol, using Rydberg tagging schemes, and compare their results to those for the photodissociation of these same two molecules in cyclohexane solution, probed using transient absorption spectroscopy.

The calculated potential energy curves[62] for the two molecules in Fig. 9 are qualitatively similar. However, the relative energies of the conical intersections differ because the $\pi\sigma^*$ state crosses the bound $\pi\pi^*$ state at a lower relative energy in *p*-methylthiophenol than in phenol. Comparing the solution and gas-phase results shows that most aspects of the initial dissociation dynamics are the same in cyclohexane solution and in an isolated molecule. As in isolated molecules, the energy of the initial excitation relative to the crossing of the $\pi\pi^*$ and $\pi\sigma^*$ states strongly

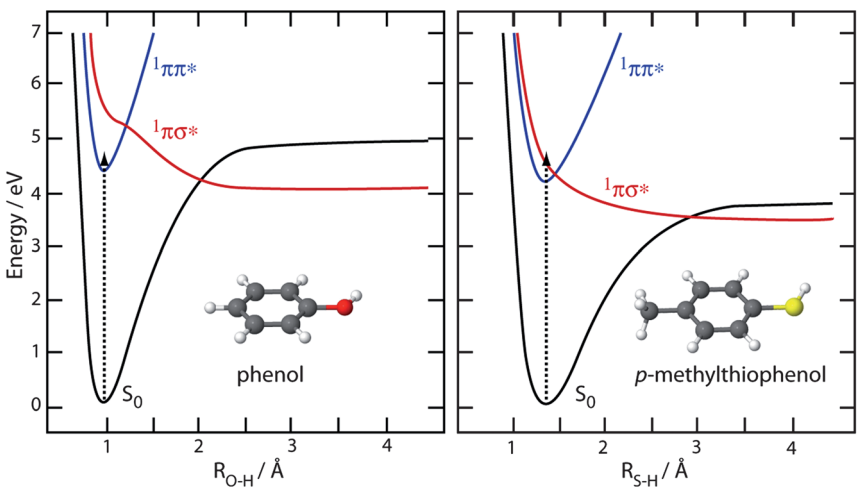

Fig. 9 Calculated potential energy curves for the first three singlet states of phenol (left) and *p*-methylthiophenol (right). The vertical dotted arrow indicates the energy of a 267-nm photon. (Adapted from ref. 62 with permission of the Royal Society of Chemistry.)

influences the dissociation dynamics. Because the dissociative $\pi\sigma^*$ state lies at a relatively low energy in *p*-methylthiophenol, excitation with a 267-nm photon leads to ultrafast dissociation for molecules both in solution and in the gas phase. However, the $\pi\sigma^*$ state lies above the energy provided by a 267-nm photon in phenol, and the ultrafast solution-phase measurements directly observe the slow dissociation in about 1 ns that state-resolved measurements suggest also occurs in the gas-phase. The dynamics are not completely indifferent to the phase in which the dissociation occurs, and hydrogen-bonded dimers and other oligomers may play a role in solution.[62]

3.3.2 Solvent-induced isomerization. The surrounding solvent can also exert more direct influence on photodissociation in solution. In the gas phase, placing a molecule in a repulsive excited state generally causes the fragments to separate unimpeded by further interactions. There are examples of roaming in isolated molecules, in which relatively direct dissociation competes with a rearrangement followed by decomposition to the same products. The common feature in these systems is the presence of a channel leading to different products that is near enough in energy to allow the system to explore that channel but not dissociate. For example, there is a radical decomposition channel for formaldehyde, $H_2CO \rightarrow H + HCO$, that facilitates roaming in the molecular dissociation channel, $H_2CO \rightarrow H_2 + CO$. In this case, the hydrogen atom that explores the radical channel returns to form H_2 in the molecular channel rather than depart completely.[69,70]

The surroundings can hinder separation of the products in solution, frustrating the dissociation and turning direct photolysis into isomerization. The most likely consequence of such caging is recombination to restore the original molecule, but if there are other stable arrangements of the atoms, it can induce isomerization into that geometry. The photolysis of halomethanes is an example.[71,72] Gas-phase photodissociation of bromoform, $CHBr_3$, cleaves the C–Br bond to produce free Br and a halomethyl radical

$$CHBr_3 \rightarrow CHBr_2 + Br$$

which separate completely. In solution, however, the departing Br atom can return to the radical and either reform bromoform or, less frequently, bind to one of the Br atoms on the radical to form *iso*-bromoform, $CHBr_2$-Br. Fig. 10(a) shows the structure of the isomer that contains a Br–Br bond. There are many examples of formation of *iso*-halomethanes, and some of them are intermediates in reactions with olefins.[73]

The ground-state potential energy surface and corresponding contour map in Fig. 10(a) show the two minima and the minimum-energy pathway between them, which passes over a barrier that lies below the dissociation asymptote. Calculations show that isomerization along this path occurs by stretching one bond to a halogen atom and swinging it around to another halogen atom.[74,75] The location of this barrier below the nearby dissociation asymptote is reminiscent of the situation that produces roaming in isolated molecules. In this case, however, interactions with the surroundings are a key component of the isomerization, which does not follow the minimum-energy path.

The upper curve in Fig. 10(b) shows the excited state of bromoform on which direct dissociation occurs in the gas phase. In solution, by contrast, the separating fragments encounter the surroundings, which provide the "cage repulsion" marked in the figure. The departing atom returns to explore new configurations including that of the isomer. We have followed this isomerization in solution using ultrafast, broadband transient infrared spectroscopy. The 30 cm^{-1} difference in the C–H stretching transitions in bromform and *iso*-bromoform allows us to follow the evolution of both species.[74] The isomer appears in less than 10 ps, and its spectrum evolves over about 100 ps as the vibrationally excited isomer relaxes.

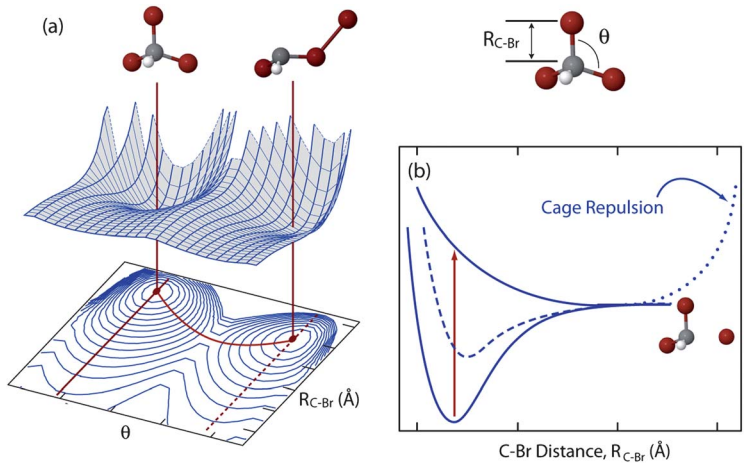

Fig. 10 (a) Sketch of the potential energy surface for ground state bromoform, $CHBr_3$. The structure in the upper right shows the coordinate system. There is a deep minimum for the bromoform (left) and a shallower minimum for the isomer, *iso*-bromoform (right). The barrier along the minmum energy path connecting the two lies below the dissociation asymptote. (b) Cuts through the ground-state surface for bromoform and *iso*-bromoform and through the excited-state surface for bromoform. The dotted curve qualitatively represents the repulsion by the surrounding molecules in solution.

4. Conclusions

Conceptual and technical advances are enabling studies of reaction dynamics in gases and liquids and at interfaces with sufficient detail to allow comparison of closely related reactions in different environment. One example described in this Discussion is the fate of methane and its isotopologues prepared in selected vibrational states. There are studies of their reactions with halogen atoms in the gas phase and of their dissociative chemisorption on a metal surface. Initial vibrational excitation influences the course of the reaction similarly, producing mode- and bond-selected chemistry in both cases. Another example is bimolecular reaction in solution, where the relative reaction rates and the energy disposal mirror analogous gas-phase reactions. The surroundings also influence photodissociation to different degrees depending on the system. In one example, the photolysis of a pair of isolated, aromatic molecules is similar to that of the same two molecules in solution, albeit with some subtle differences arising from solvation. For those two molecules, the energy at which there is a conical intersection between two excited states is the dominant factor in both environments. By contrast, there are examples where the surroundings exert a much stronger influence by inhibiting the separation of fragments and producing isomers. The key to all of these studies is examining systems in sufficient detail in multiple environments to permit detailed comparisons. As the contributions to this Discussion illustrate, increasingly sophisticated experimental approaches and theoretical descriptions open the door to ever more incisive studies in increasing complex systems.

Acknowledgements

The U.S. National Science Foundation and the U.S. Department of Energy sponsor different aspects of the work from the University of Wisconsin - Madison described here. The National Science Foundation (CHE-0910917) supports the research on bimolecular reactions of translationally and vibrationally energized molecules in the gas-phase and the research on bimolecular reactions and cage recombination

in solution. The Office of Basic Energy Sciences of the Department of Energy (DE-FG02-86ER13500) supports the research on photodissociation of vibrationally excited molecules.

References

1 D. R. Yarkony, *Acc. Chem. Res.*, 1998, **31**, 511–518.
2 H. A. Kramers, *Physica*, 1940, **7**, 284–304.
3 R. F. Grote and J. T. Hynes, *J. Chem. Phys.*, 1980, **73**, 2715–2732.
4 J. C. Polanyi, *Acc. Chem. Res.*, 1972, **5**, 161–168.
5 F. F. Crim, *Proc. Natl. Acad. Sci. U. S. A.*, 2008, **105**, 12654–12661.
6 G. Czako and J. M. Bowman, *J. Chem. Phys.*, 2012, **136**, 044307.
7 M. Cheng, Y. Feng, Y. K. Du, Q. H. Zhu, W. J. Zheng, G. Czako and J. M. Bowman, *J. Chem. Phys.*, 2011, **134**, 191102.
8 H. Kawamata, W. Zhang and K. Liu, *Faraday Discussions*, 2012, **157**, DOI: 10.1039/C2FD20004J.
9 W. R. Simpson, A. J. Orr-Ewing and R. N. Zare, *Chem. Phys. Lett.*, 1993, **212**, 163–171.
10 H. Kawamata and K. P. Liu, *J. Chem. Phys.*, 2010, **133**, 124304.
11 A. E. Berke, E. H. Volpa and F. F. Crim, *J. Phys. Chem. A*, 2012, (in preparation).
12 M. S. Child and L. Halonen, *Adv. Chem. Phys.*, 1984, **57**, 1–58.
13 M. S. Child, *Acc. Chem. Res.*, 1985, **18**, 45–50.
14 S. Yoon, S. Henton, A. N. Zivkovic and F. F. Crim, *J. Chem. Phys.*, 2002, **116**, 10744–10752.
15 S. Yoon, R. J. Holiday and F. F. Crim, *J. Chem. Phys.*, 2003, **119**, 4755–4761.
16 S. Yoon, R. J. Holiday, E. L. Sibert and F. F. Crim, *J. Chem. Phys.*, 2003, **119**, 9568–9575.
17 A. E. Berke, C. J. Annesley, E. H. Volpa and F. F. Crim, *J. Phys. Chem. A*, 2012, (in preparation).
18 W. J. van der Zande, R. Zhang, R. N. Zare, K. G. McKendrick and J. J. Valentini, *J. Phys. Chem.*, 1991, **95**, 8205.
19 A. E. Berke, Ph.D., University of Wisconsin - Madison, 2012.
20 R. J. Holiday, C. H. Kwon, C. J. Annesley and F. F. Crim, *J. Chem. Phys.*, 2006, **125**, 133101.
21 C. J. Annesley, A. E. Berke and F. F. Crim, *J. Phys. Chem. A*, 2008, **112**, 9448–9453.
22 S. Yan, Y. T. Wu, B. L. Zhang, X. F. Yue and K. P. Liu, *Science*, 2007, **316**, 1723–1726.
23 J. R. Fair, D. Schaefer, R. Kosloff and D. J. Nesbitt, *J. Chem. Phys.*, 2002, **116**, 1406–1416.
24 L. Halonen, S. L. Bernasek and D. J. Nesbitt, *J. Chem. Phys.*, 2001, **115**, 5611–5619.
25 A. Sinha, M. C. Hsiao and F. F. Crim, *J. Chem. Phys.*, 1991, **94**, 4928–4935.
26 A. Sinha, J. D. Thoemke and F. F. Crim, *J. Chem. Phys.*, 1992, **96**, 372–376.
27 J. D. Thoemke, J. M. Pfeiffer, R. B. Metz and F. F. Crim, *J. Phys. Chem.*, 1995, **99**, 13748–13754.
28 D. Raftery, M. Iannone, C. M. Phillips and R. M. Hochstrasser, *Chem. Phys. Lett.*, 1993, **201**, 513–520.
29 D. Raftery, E. Gooding, A. Romanovsky and R. M. Hochstrasser, *J. Chem. Phys.*, 1994, **101**, 8572–8579.
30 L. Sheps, A. C. Crowther, S. L. Carrier and F. F. Crim, *J. Phys. Chem. A*, 2006, **110**, 3087–3092.
31 L. Sheps, A. C. Crowther, C. G. Elles and F. F. Crim, *J. Phys. Chem. A*, 2005, **109**, 4296–4302.
32 S. M. Aschmann and R. Atkinson, *Int. J. Chem. Kinet.*, 1995, **27**, 613–622.
33 S. M. Senkan and D. Quam, *J. Phys. Chem.*, 1992, **96**, 10837–10842.
34 G. A. Bethardy, F. J. Northrup and R. G. Macdonald, *J. Chem. Phys.*, 1996, **105**, 4533–4549.
35 L. R. Copeland, F. Mohammad, M. Zahedi, D. H. Volman and W. M. Jackson, *J. Chem. Phys.*, 1992, **96**, 5817.
36 V. R. Morris, F. Mohammad, L. Valdry and W. M. Jackson, *Chem. Phys. Lett.*, 1994, **220**, 448–454.
37 S. J. Greaves, R. A. Rose, T. A. A. Oliver, D. R. Glowacki, M. N. R. Ashfold, J. N. Harvey, I. P. Clark, G. M. Greetham, A. W. Parker, M. Towrie and A. J. Orr-Ewing, *Science*, 2011, **331**, 1423–1426.
38 R. A. Rose, S. J. Greaves, T. A. A. Oliver, I. P. Clark, G. M. Greetham, A. W. Parker, M. Towrie and A. J. Orr-Ewing, *J. Chem. Phys.*, 2011, **134**, 244503.
39 A. C. Crowther, S. L. Carrier, T. J. Preston and F. F. Crim, *J. Phys. Chem. A*, 2008, **112**, 12081–12089.

40 L. B. F. Juurlink, P. R. McCabe, R. R. Smith, C. L. DiCologero and A. L. Utz, *Phys. Rev. Lett.*, 1999, **83**, 868–871.
41 L. B. F. Juurlink, R. R. Smith and A. L. Utz, *Faraday Discuss.*, 2000, **117**, 147–160.
42 L. B. F. Juurlink, R. R. Smith and A. L. Utz, *J. Phys. Chem. B*, 2000, **104**, 3327–3336.
43 R. R. Smith, D. R. Killelea, D. F. DelSesto and A. L. Utz, *Science*, 2004, **304**, 992–995.
44 L. B. F. Juurlink, R. R. Smith, D. R. Killelea and A. L. Utz, *Phys. Rev. Lett.*, 2005, **94**, 208303.
45 D. R. Killelea, V. L. Campbell, N. S. Shuman and A. L. Utz, *Science*, 2008, **319**, 790–793.
46 D. R. Killelea, V. L. Campbell, N. S. Shuman and A. L. Utz, *J. Phys. Chem. C*, 2008, **112**, 9822–9827.
47 R. D. Beck, P. Maroni, D. C. Papageorgopoulos, T. T. Dang, M. P. Schmid and T. R. Rizzo, *Science*, 2003, **302**, 98–100.
48 P. Maroni, D. C. Papageorgopoulos, M. Sacchi, T. T. Dang, R. D. Beck and T. R. Rizzo, *Phys. Rev. Lett.*, 2005, **94**, 246104.
49 R. Bisson, M. Sacchi, T. T. Dang, B. Yoder, P. Maroni and R. D. Beck, *J. Phys. Chem. A*, 2007, **111**, 12679–12683.
50 R. Bisson, M. Sacchi and R. D. Beck, *J. Chem. Phys.*, 2010, **132**, 094702.
51 R. Bisson, M. Sacchi and R. D. Beck, *Phys. Rev. B: Condens. Matter Mater. Phys.*, 2010, **82**, 121404.
52 B. L. Yoder, R. Bisson and R. D. Beck, *Science*, 2010, **329**, 553–556.
53 J. Higgins, A. Conjusteau, G. Scoles and S. L. Bernasek, *J. Chem. Phys.*, 2001, **114**, 5277–5283.
54 L. Chen, H. Ueta, R. Bisson and R. D. Beck, *Faraday Discussions*, 2012, **157**, DOI: 10.1039/C2FD20007D.
55 F. Bernardi, M. Olivucci and M. A. Robb, *Chem. Soc. Rev.*, 1996, **25**, 321–328.
56 D. R. Yarkony, *J. Phys. Chem. A*, 2001, **105**, 6277–6293.
57 W. Domcke, L. Seidner and G. Stock, *Springer Ser. Chem. Phys.*, 1998, **63**, 491–495.
58 B. G. Levine and T. J. Martinez, *Annu. Rev. Phys. Chem.*, 2007, **58**, 613–634.
59 M. N. R. Ashfold, B. Cronin, A. L. Devine, R. N. Dixon and M. G. D. Nix, *Science*, 2006, **312**, 1637–1640.
60 Z. G. Lan, W. Domcke, V. Vallet, A. L. Sobolewski and S. Mahapatra, *J. Chem. Phys.*, 2005, **122**, 224315.
61 A. L. Sobolewski and W. Domcke, *J. Phys. Chem. A*, 2001, **105**, 9275–9283.
62 Y. Zhang, T. A. A. Oliver, M. N. R. Ashfold and S. E. Bradforth, *Faraday Discussions*, 2012, **157**, DOI: 10.1039/C2FD20043K.
63 G. de Wit, B. R. Heazlewood, M. S. Quinn, A. T. Maccarone, K. Nauta, S. A. Reid, M. J. T. Jordan and S. H. Kable, *Faraday Discussions*, 2012, **157**, DOI: 10.1039/C2FD20015E.
64 R. L. Vander Wal, J. L. Scott and F. F. Crim, *J. Chem. Phys.*, 1990, **92**, 803.
65 A. Bach, J. M. Hutchison, R. J. Holiday and F. F. Crim, *J. Phys. Chem. A*, 2003, **107**, 10490–10496.
66 M. L. Hause, Y. H. Yoon and F. F. Crim, *J. Chem. Phys.*, 2006, **125**, 174309.
67 D. R. Yarkony, *J. Chem. Phys.*, 2004, **121**, 628–631.
68 M. L. Hause, Y. H. Yoon, A. S. Case and F. F. Crim, *J. Chem. Phys.*, 2008, **128**, 104307.
69 J. M. Bowman and B. C. Shepler, *Annu. Rev. Phys. Chem.*, 2011, **62**, 531–553.
70 N. Herath and A. G. Suits, *J. Phys. Chem. Lett.*, 2011, **2**, 642–647.
71 X. Zheng, W.-H. Fang and D. L. Phillips, *J. Chem. Phys.*, 2000, **113**, 10934–10946.
72 X. M. Zheng and D. L. Phillips, *Chem. Phys. Lett.*, 2000, **324**, 175–182.
73 D. L. Phillips, W. H. Fang, X. Zheng, Y. L. Li, D. Wang and W. M. Kwok, *Curr. Org. Chem.*, 2004, **8**, 739–755.
74 T. J. Preston, M. A. Shaloski and F. F. Crim, 2012, (in preparation).
75 T. J. Preston, Ph.D., University of Wisconsin - Madison, 2012.

